





**Pair interaction of localized topological structures in confined chiral media**I. M. Tambovtsev <sup>1,2,3</sup>, I. S. Lobanov <sup>1</sup>, Alexei D. Kiselev <sup>4</sup>, and V. M. Uzdin <sup>1,2</sup><sup>1</sup>*Faculty of Physics, ITMO University, 197101 St. Petersburg, Russia*<sup>2</sup>*Department of Physics, St. Petersburg State University, St. Petersburg 198504, Russia*<sup>3</sup>*Science Institute and Faculty of Physical Sciences, University of Iceland, 107 Reykjavik, Iceland*<sup>4</sup>*Laboratory of Quantum Processes and Measurements, ITMO University, 199034 Saint Petersburg, Russia*

(Received 15 May 2023; accepted 8 August 2023; published 31 August 2023)

We study pairwise interactions between localized topological structures in chiral magnetic and cholesteric liquid crystal (CLC) systems confined in the planar geometry. Our calculations for magnetics are based on the lattice model that takes into account the bulk and surface anisotropies along with the exchange and the Dzyaloshinskii-Moriya interactions. In CLC cells, these anisotropies describe the energy of interaction with an external magnetic or electric field and the anchoring energy assuming that the magnetic or electric anisotropy is negative and the boundary conditions are homeotropic. We have selected the region of the phase diagram, where various localized solitonlike structures, including skyrmion tubes, torons, and leeches, embedded in the ground state of the  $z$ -cone (conical phase) coexist, and carried out numerical analysis of the distance dependencies of the effective intersoliton interaction potentials. For skyrmions and torons, the potentials are found to be attractive in the large separation region. It turned out that for these potentials, the effects of axial asymmetry are negligible. By contrast, it turned out that for the intermediate structures between the skyrmions and torons known as the leeches, the leech-leech potentials generally depend on the orientation of the intersoliton separation vector and their large distance parts may become repulsive at certain directions of the vector. All the potentials have the short distance repulsive parts and the local minima located at the equilibrium separations. It is found that the skyrmion-skyrmion potential has an additional metastable configuration shifted towards the short-distance region.

DOI: [10.1103/PhysRevE.108.024705](https://doi.org/10.1103/PhysRevE.108.024705)**I. INTRODUCTION**

Magnets, liquid crystals (LCs), and colloids are known as host materials for numerous topological solitons such as skyrmions, antiskyrmions, torons, bobbers, hopfions, heliknotons, and twistions [1–9]. In the zoo of solitons, the skyrmions represent one of the most studied structures that are promising for a new generation of racetrack memories and a wealth of spintronic and photonic applications [10–14]. Under certain conditions, especially in three-dimensional systems, different localized topological structures can coexist [15].

There are chiral materials such as chiral magnets and chiral nematic liquid crystals, also known as cholesteric liquid crystals (CLCs), that have attracted particular interest as systems providing valuable insights into the above diversity of localized structures [8,15–18]. The chirality of magnetic materials is typically due to the Dzyaloshinskii-Moriya interaction (DMI) caused by the spin-orbit coupling, whereas chiral ordering observed in CLCs is an immediate consequence of the broken mirror symmetry caused by the presence of anisotropic molecules with no mirror plane. An important point is that the bulk chirality of CLC materials, which is typically determined by the concentration of chiral additives, can be controlled by external stimuli such as temperature, electromagnetic fields, and the anchoring conditions at boundary surfaces [19–23]. The latter is closely related to the size and type of the confined geometry, which is another important factor that may greatly influence localized structures in both chiral magnetic and CLC systems.

In thin chiral magnetic films, the quasi-two-dimensional skyrmions can appear either as individual objects or as skyrmion lattices [24]. In magnetic systems that are a few atomic monolayers thick, these topological solitons are uniform along the normal to the film [3]. By contrast, in bulk chiral media, one can observe extended skyrmion tubes with discrete translational symmetry along the tube. Thus, these structures are not completely homogeneous along these lines [25].

In the bulk of chiral ferromagnets, at external magnetic fields in a certain range, the ground state is the cone phase with the cone axis along the magnetic field [26]. Such systems may also contain metastable asymmetric skyrmions. In the slab geometry, the cone ground state and metastable skyrmions can be realized in LC cells with homeotropic anchoring of the director at the substrates [15,27]. When the cell thickness compares with the equilibrium pitch of the bulk helical ground-state structure, additional localized structures such as torons and leeches can be implemented [15].

Although localized topological structures in chiral media behave like separate quasiparticles, they interact and this interaction determines the geometry of many-soliton structures, as well as their collective dynamics and properties.

In the two-dimensional case, magnetic skyrmions tend to repel each other, but this interaction decreases exponentially with the interskyrmion distance [18,28–30]. The repulsion is determined by the change in DMI, which makes a negative contribution to the self-energy of a single skyrmion. However,

in metal films with frustrated exchange interaction, at certain distances between skyrmions, effective attractive interactions may occur, leading to the formation of skyrmion clusters [31].

In three-dimensional systems, skyrmion tubes can be attracted to each other and form quite complex topological structures. In Refs. [32,33], it was found that skyrmion tubes perturb the surrounding chiral environment, leading to the formation of complex superstructures that contain both parallel and orthogonal tubes. The tubes can be deformed when they are separated by the distance of the order of their diameter.

Direct observation of attractive skyrmions and skyrmion clusters in the conical phase of the cubic  $\text{Cu}_2\text{OSeO}_3$  helimagnet was reported by Loudon *et al.* in Ref. [34]. In B20-type FeGe strips, the skyrmion attraction was also observed at moderate magnetic fields. The attraction is found to change into repulsion as the field increases [35].

In bulk chiral materials, the structure of the skyrmion clusters can be rather complex and can be controlled using an external magnetic field. Skyrmion tubes can be located either perpendicular or parallel to the external magnetic field, and such configurations coexist in a specific range of fields [25,32]. A similar complex configuration of skyrmion tubes has been predicted and observed in chiral LC systems [33]. The crossover between different regimes of skyrmion interaction has been revealed by changing the layer thickness and/or the surface anchoring.

Interestingly, topological particlelike localized LC structures bear some resemblance to colloidal particles dispersed in a LC host (see reviews [6,36,37] for details on liquid crystal colloids). Colloidal interactions are mediated by elastic distortions induced by the interacting particles [38–46]. When the characteristic length of the distortions is larger than the particles' size, the elastic interaction can be approximately described using an analogy with the interaction between electrostatic multipoles [47]. Otherwise, the confined geometry and the anchoring conditions may have a profound effect on the colloidal interactions [44–46].

Similar to interparticle interaction in LC colloids, the interskyrmion interaction in CLCs is determined by the elastic interactions [48]. These interactions can also be tuned by an external electric field [49].

In magnetic films, the properties of localized magnetic structures such as skyrmion tubes depend on the film thickness [50]. In thin films, new localized topological structures can be stabilized near the surfaces and interfaces of magnetic and LC-chiral media [15]. These include chiral bobbles experimentally observed in thin plates of B20-type FeGe [16], stacked spin spirals in magnetic films [51], torons, twisted walls, fingers, and their hybrids in chiral nematics [52].

Interaction between such structures is much less studied as compared to the interskyrmion interaction in the bulk. In this paper, the intersoliton interaction between topological structures formed in the films filled with chiral magnetic and LC media will be our primary concern.

The paper is organized as follows. In Sec. II, we describe the model and the soliton structures simultaneously stabilized in the coexistence region of the phase diagram. The numerical procedure employed for computing the intersoliton interaction potentials is outlined in Sec. III, where we also present the results of our calculations. Three-soliton structures are briefly

discussed in Sec. IV. Finally, in Sec. V, we draw our results together and make some concluding remarks.

## II. MODEL AND LOCALIZED STRUCTURES

Following our previous study [15], we consider a chiral magnetic and nematic liquid crystal material confined in the slab geometry and begin with the continuum model of the film giving the free energy functional of the following form:

$$F[\mathbf{m}] = \int_V dV \{ \mathcal{A}(\nabla\mathbf{m})^2 - \mathcal{D}\mathbf{m} \cdot [\nabla \times \mathbf{m}] - \mathcal{K}_b(\mathbf{m} \cdot \mathbf{z})^2 \} - \mathcal{K}_s \int_S ds (\mathbf{m} \cdot \mathbf{z})^2, \quad (1)$$

where  $V$  is the volume of the film and  $S$  is the bounding surface represented by two substrates normal to the  $z$  axis;  $\mathbf{m}(\mathbf{r})$  is the vector field representing either the unit magnetization vector or the CLC director; and  $\mathbf{z}$  is the unit vector along the anisotropy axis assumed to be normal to the bounding surfaces  $S$ .

For magnetic systems, the first term describes the exchange interaction determined by the exchange stiffness  $\mathcal{A}$ , which is assumed to be homogeneous in the bulk of the film. The second term corresponds to chiral Dzyaloshinskii-Moriya interaction (DMI) with the interaction constant  $\mathcal{D}$ . The third contribution is the density of magnetic anisotropy described by the parameter  $\mathcal{K}$ , whose values inside the film,  $\mathcal{K} = \mathcal{K}_b$ , and at its boundaries may differ,  $\mathcal{K}_s \neq \mathcal{K}_b$ .

For LC systems, the value of  $\mathcal{A}$  and the chiral interaction constant  $\mathcal{D}$  are expressed in terms of the Oseen-Frank moduli in the one-constant approximation where all the elastic constants are assumed to be equal,  $K_1 = K_2 = K_3 = K$ :  $\mathcal{A} = K/2$  and  $\mathcal{D} = Kq_0$ , where  $q_0$  is the free twisting wave number. In this case, the bulk value of the anisotropy constant,  $\mathcal{K}_b$ , plays the role of the coupling constant for interaction with the external magnetic field, whereas its value at the substrates corresponds to the anchoring energy strength (the anchoring conditions are assumed to be homeotropic).

As in Ref. [15], our overall computational strategy involves two basic steps: (a) we introduce a properly discretized version of the free energy (1) as the lattice model of the Heisenberg-like form on the rectangular three-dimensional (3D) grid of the size  $N_x \times N_y \times N_z$ , and (b) we employ the direct energy minimization by the nonlinear conjugate gradient method in Cartesian coordinates with constraints that fix the unit length of the magnetization or director at the sites of the lattice.

For the lattice model with magnetic moments or CLC directors localized at the sites of a simple cubic lattice, the energy of the system reads [15]

$$E[\mathbf{S}] = - \sum_{\langle i,j \rangle} (J\mathbf{S}_i \cdot \mathbf{S}_j + \mathbf{D}_{i,j} \cdot [\mathbf{S}_i \times \mathbf{S}_j]) - \sum_i K_i (S_i^z)^2, \quad (2)$$

where summation  $\langle i, j \rangle$  is performed over the nearest neighbors,  $J = 2a\mathcal{A}$  is the exchange parameter,  $\mathbf{D}_{ij}$  is the DMI vector of the length  $|\mathbf{D}_{ij}| \equiv D = a^2\mathcal{D}$ , and  $K_{b,s} = a^2\mathcal{K}_{b,s}$  is the anisotropy parameter;  $a$  is the lattice constant and  $\mathbf{S}_i \equiv \mathbf{m}_i$  is the unit vector along the magnetic moment or CLC director

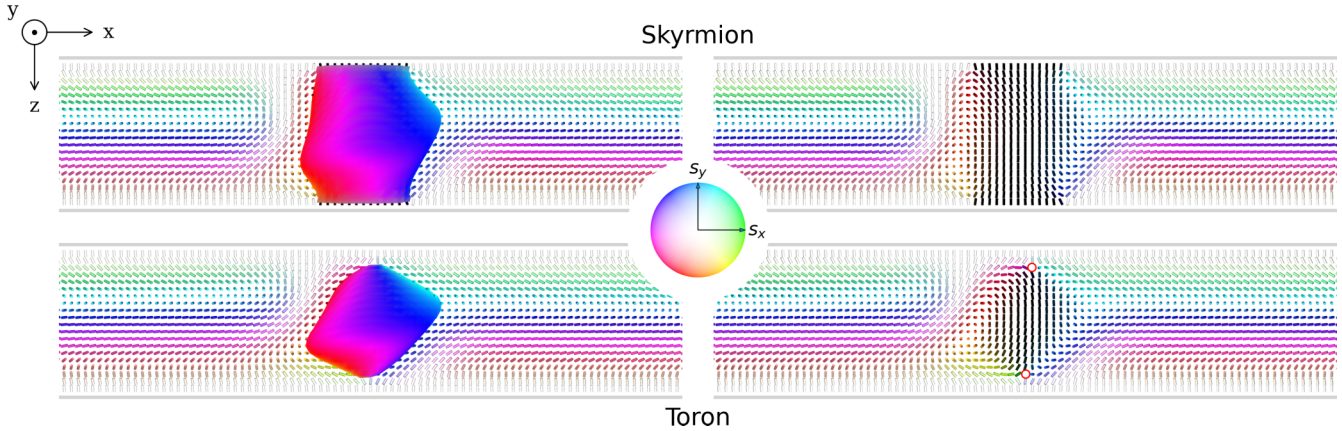


FIG. 1. Orientational structures in the  $xz$  plane for a skyrmion (top) and a toron (bottom) embedded into the film filled with chiral magnetic or LC material. The film thickness is  $p_0$  and horizontal gray lines indicate planar confining surfaces with homeotropic anchoring conditions. The magnetization or LC director field,  $\mathbf{S}$ , is shown using rods colored according to the color palette in the inset at the center that describes the  $x$  and  $y$  projections of  $\mathbf{S}$ . This color wheel represents the northern hemisphere of magnetization or director orientations where  $S_z$  is non-negative and the white color represents the direction along the  $z$  axis with  $S_z = 1$ . In the southern hemisphere, the colors become darker as  $S_z$  decreases, approaching the southern pole with  $S_z = -1$  indicated by black color. The surfaces on the left are isosurfaces of the  $z$  projection of  $\mathbf{S}$  computed at  $S_z = 0$  for the skyrmion (top) and the toron (bottom) structures, whose orientational fields are depicted on the right side of the figure. Circles indicate two point defects (hedgehogs) in the toron structure.

at the site  $i$ . For the sake of brevity, the vectors  $\mathbf{S}_i$  representing the unit magnetization vector or CLC director are sometimes loosely called the spins.

Similar to the continuum model (1), the first term on the right-hand side of Eq. (2) describes the exchange interaction, whereas the second term is DMI. Both the exchange parameter  $J$  and the length of the DMI vector,  $\mathbf{D}_{ij}$ ,  $|\mathbf{D}_{ij}| = D$ , are assumed to be constant. The direction of the DMI vector  $\mathbf{D}_{ij}$  is along the vector connecting the nodes  $i$  and  $j$ , thus stabilizing the Bloch-type skyrmion structures.

The last term in the energy (2) represents the magnetic anisotropy with the anisotropy axis normal to the substrates (the  $z$  axis). For the easy-plane anisotropy, the bulk value of  $K_i$  is negative,  $K_i = K_b \leq 0$ , and is fixed for all layers of the film. In magnetic systems, such anisotropy can be induced, for example, by magnetostatic interactions due to the flat shape of the sample [53]. We assume that owing to the additional surface anisotropy  $K_s > 0$ , the anisotropy parameter at the interfacial layers,  $K_i = K_b + K_s$ , is positive.

For LC systems, the spin  $\mathbf{S}_i$  gives vectorization of the CLC director field at the  $i$ th site and the exchange constant  $J$  is proportional to the Frank elastic constant:  $J = aK$ . The easy-plane anisotropy in the bulk corresponds to the energy of interaction between a LC with negative magnetic susceptibility,  $\Delta\chi < 0$ , and a magnetic field applied across the cell, whereas the surface anisotropy with the positive anisotropy parameter describes the surface energy for the CLC with the homeotropic anchoring conditions at bounding surfaces. The CLC chirality is characterized by the equilibrium twist wave number  $q_0 = 2\pi/p_0 = \arctan(D/J)$ , where  $p_0$  is the pitch of the helical structure representing the ground state in an unbounded sample.

It is convenient to introduce dimensionless parameters:  $\kappa^b = K_b J/D^2$  and  $\kappa^s = K_s J/D^2$ . For states homogeneous along the  $y$  axis, the phase diagram in the  $\kappa^b$ - $\kappa^s$  plane was calculated in Ref. [15]. According to this diagram, the ground

state can be represented by various types of delocalized structures, such as the  $z$ -helix, the  $z$ -cone, the  $x$ -helicoid, and the oblique helicoid depending on the dimensionless parameters of bulk and surface anisotropy,  $\kappa^b$  and  $\kappa^s$ .

It was shown that for sufficiently large values of the surface anisotropy  $\kappa^s$ , the ground state of the chiral film is the conical phase which is invariant with respect to in-plane translations and is described by the  $z$ -cone structure. Several localized topological structures can be embedded into the  $z$ -cone far-field background in the form of metastable excitations [15]. Figures 1 and 2 present some of these states, which can be regarded as topological solitons.

Orientational structures for the skyrmion tube and the toron in the cell geometry are depicted in Fig. 1. The skyrmion tube shown in Fig. 1 (top) resembles skyrmion tubes in bulk chiral magnets in a vertically aligned magnetic field [25,32]. In moderate magnetic field, the magnetically induced conical phase is found to impose a twisting effect on the tube, leading to the crankshaft structure.

Figure 1 (bottom) presents the solitonic structure that, following notations of Refs. [8,52], can be identified as the toron. This structure is essentially a skyrmion tube terminated on two point defects (hedgehogs of opposite charge) near the substrates, whereas the remaining part of the toron is localized in the bulk of the film. Although the toron in Fig. 1 (bottom) bears a general resemblance to those described in [8,52], in our case, it is surrounded by the conical phase that, similar to the skyrmion tube, induces twists of the toron.

The solitonic structure shown in Fig. 2 can be viewed as the intermediate case between the skyrmion tube and the toron and will be called the leech [15]. In asymmetric LC cells, the leechlike structures were previously described as skyrmion or toron hybrids [5,52]. By contrast to the hybrids, the leech structures under consideration are embedded into the twisted conical background of symmetric cells.



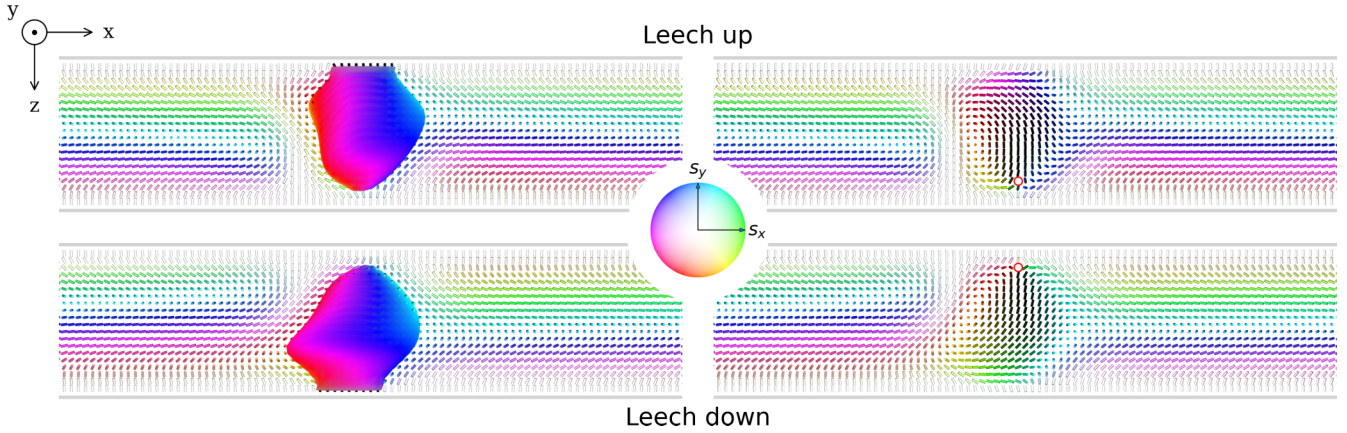


FIG. 2. Orientational structures in the  $xz$  plane for the leech up (top) and the leech down (bottom) representing the leeches that terminate on the point defects located near the upper and lower bounding surfaces, respectively (parameters and colors are described in the caption of Fig. 1).

From Fig. 2, these structures are attached to one of the substrates and terminate on a singular point near the other substrate. When the terminating point defect is located close to the upper (lower) bounding surface, the leech will be referred to as the leech up (leech down).

The regions of stability for these states are generally different. As the bulk anisotropy (external field) increases, the skyrmion tube decays into a pair of bobbers, whereas the leech and the toron will transform into a single bobber and the  $z$ -cone, respectively.

An important point is that there is the range of anisotropy parameters where all the above structures can coexist simultaneously. In this coexistence range of the phase diagram (see Fig. 14 in Ref. [15]), we shall study the intersoliton interaction between different topological structures.

In Figs. 1 and 2 and in our subsequent calculations, the values of the surface and bulk anisotropies are taken to be  $\kappa^s = 24$  and  $\kappa^b = -0.25$ , respectively. These values correspond to the point in the coexistence domain of the phase diagram. We shall also assume that the film thickness equals the equilibrium pitch  $p_0 = N_z a$ , where  $a$  is the lattice constant and  $N_z = 20$ , and thus the DMI parameter (the length of the DMI vector) is  $D = J \tan(\pi/10)$ . The in-plane (lateral) size of the film with the boundary surfaces (substrates) parallel to the  $x$ - $y$  plane is  $N_x \times N_y = 400 \times 400$  and the in-plane boundary conditions are periodic.

### III. PAIRWISE INTERSOLITON INTERACTIONS

In this section, we study the interactions between the localized topological (soliton) structures depicted in Figs. 1 and 2. Orientational distributions for these structures computed using the parameters listed at the end of the preceding section can now be used to produce the initial seed states for two-soliton configurations spaced at a given intersoliton distance. More specifically, the initial configurations are obtained by placing two cutouts from single-soliton textures in the nonoverlapping cylinder-shaped domains of the radius equal to  $7.5a$  into the background structure without topological solitons.

Each seed state is subjected to the three-step minimization procedure. During the first step, orientation of two magnetic moments or CLC directors (spins) located at the centers of interacting solitons are kept intact and the initial structure is optimized to achieve a local energy minimum under the above constraint that fixes the intersoliton separation. At the second step, in order to reduce the error in estimated energy arising due to the presence of frozen (pinned) spins, a minimization procedure is applied so as to correct the orientation of the magnetic moments or CLC directors (spins) in close vicinity of the pinned spins, including themselves (the radius of the neighborhood is  $5a$ ). This step ensures that the spins outside the neighborhood remain unchanged. Finally, the minimization procedure used at the first step is repeated. This procedure can be continued iteratively, but calculations show that the difference between the energies evaluated at the last two steps is negligibly small. So, changes in energy are mainly produced by minimization performed at the second step. Note that our approach can be employed to improve the accuracy of the calculations of the skyrmion-skyrmion and skyrmion-defect interactions performed in Refs. [29,54,55], where the distances are fixed using the fixed center-spin method corresponding to the first step of our procedure.

Note that at sufficiently large distances, additional unconstrained minimization of the optimized structure will not produce noticeable changes in the loci of the solitons. This is the lattice (discretization) effect that manifests itself in the presence of numerous nearly degenerate metastable configurations on the energy surface.

The above numerical procedure is applied to compute the energy of the two-soliton structures as a function of the distance between the solitons. The difference between this energy and the sum of single-soliton energies gives the interaction energy. In order to reduce numerical error caused by subtraction of large energies resulting from a huge number of spins, the energies were counted from the cone ground state.

Note that the intersoliton separation is determined by the vector connecting the centers of the solitons evaluated using the procedure that bears close similarity to evaluating the center of mass. In this procedure, the weight of the  $i$ th point is



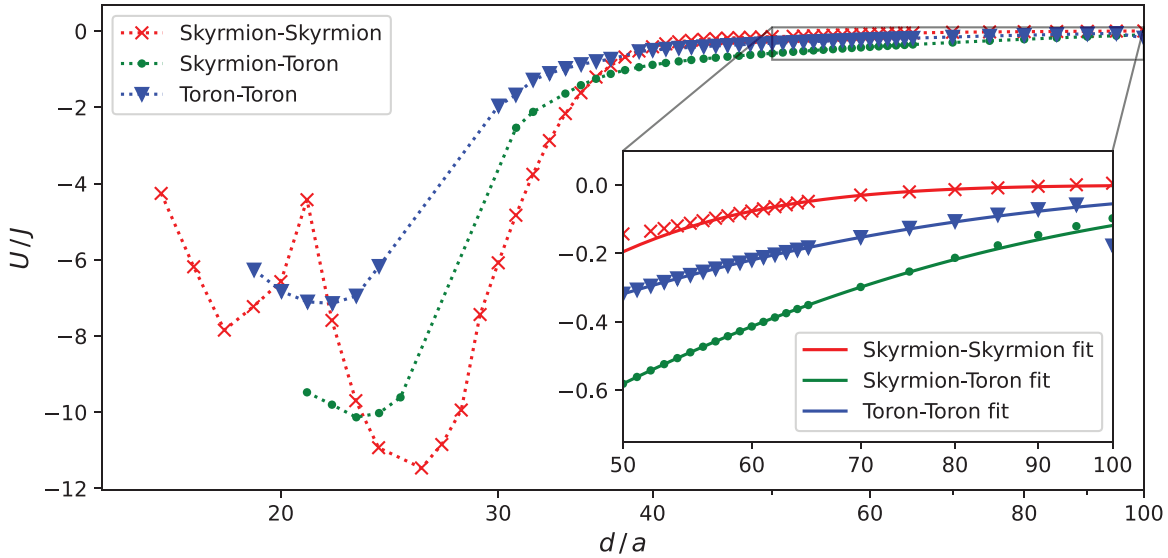


FIG. 3. Dependence of effective potentials of pairwise interactions between skyrmions and torons on dimensionless intersoliton separation,  $d/a$ . The inset enlarges the long-separation tails of the potentials fitted assuming that their large-distance asymptotic behavior is described by formula (3). Solid lines are the fitting curves computed at the values of the decay rate fitting parameter:  $c_2 = 0.0282$  (the toron-toron interaction),  $c_2 = 0.0847$  (the skyrmion-skyrmion interaction), and  $c_2 = 0.0249$  (the toron-skyrmion interaction).

the length of difference between the local spin (magnetization, LC director)  $\mathbf{S}_i$  and the corresponding vector  $\mathbf{S}_i^{(\text{cone})}$  specifying the orientation of the unperturbed background structure:  $|\mathbf{S}_i - \mathbf{S}_i^{(\text{cone})}|$ .

Figure 3 shows the results for the dependence of the interaction energy on the separation  $d$  computed for different pairs: a pair of skyrmion tubes (S-S), a pair of torons (T-T), and a toron-skyrmion tube pair (T-S). It can be seen that at large separations, skyrmions and torons are attracted to each other.

According to theoretical studies on the pair interaction between 2D skyrmions [18,28–30], the asymptotic behavior of interskyrmion potentials is described by the relation

$$U(d) \approx \frac{c_1}{\sqrt{d}} \exp(-c_2 d). \quad (3)$$

Note that for 3D skyrmions, this result also follows from the theoretical considerations of Ref. [48], where the skyrmions were viewed as colloidal particles and the interskyrmion interaction was treated as an elastic interaction between colloidal particles. According to Ref. [43], formula (3) also governs the long-distance regime of the interparticle potential for colloidal particles in a nematic cell with rigid homeotropic anchoring conditions.

We have used Eq. (3) to fit large-distance tails of the potentials using coefficients  $c_1$  and  $c_2$  as the fitting parameters. The results presented in the inset of Fig. 3 show that in the large-separation range, the asymptotics given by formula (3) provide a good approximation for intersolitic interactions involving skyrmions and torons. Specifically, the toron-toron interaction potential with  $c_2 = 0.0282$  is found to decay slower than both the interskyrmion ( $c_2 = 0.0847$ ) and the skyrmion-toron ( $c_2 = 0.0249$ ) potentials. The coefficients in the asymptotics are computed for the parameters specified above.

Referring to Fig. 3, at small distances of the order of the size of topological solitons, the particlelike structures repel each other and, for each interaction potential, there is a minimum intersoliton distance  $d_{\text{min}}$  giving the equilibrium separation of the most energetically favorable two-soliton configuration. Clearly, our considerations are not applicable to the region of intersoliton separations that are smaller than the soliton size, where orientational structures are significantly disturbed, forming new complex states.

As can be seen from Fig. 3, the minimum distances are ordered as follows:  $d_{\text{min}}^{(T-T)} < d_{\text{min}}^{(T-S)} < d_{\text{min}}^{(S-S)}$ . Thus, the largest minimum distance corresponds to the two-skyrmion structure, whereas the pair of torons possess the shortest equilibrium separation. The potential well for the bounded pair is deeper for solitons with larger separations, so the two-skyrmion pair is the most stable configuration, whereas the pair of torons is the least stable one. Interestingly, the two-skyrmion potential exhibits two local minima at the distances  $d = 18a$  and  $d = 26a$ , where the latter represents the equilibrium structure with the lowest energy (Fig. 3).

In the vicinity of the minimum, the distance dependence of the interaction energy is parabolic and can be described in terms of the stiffness of the effective interaction  $k$ . From Fig. 3, it is clear that as opposed to the case of the minimum distances, the largest stiffness  $k_{T-T}$  corresponds to the pair of torons, whereas a couple of skyrmion tubes has the smallest stiffness,  $k_{S-S}$ . So, we have  $k_{T-T} > k_{T-S} > k_{S-S}$ .

The existence of the minima for the pair interaction potentials would result in the formation of spatially ordered structures such as two-dimensional clusters, similar to the schools of skyrmions observed in CLC films [49]. The above three equilibrium two-soliton structures are shown in Fig. 4. The values of the effective potential at local minima corresponding to these structures give two-soliton binding (bonding) energies. For skyrmions and torons, these energies are listed in the first column of Table I.

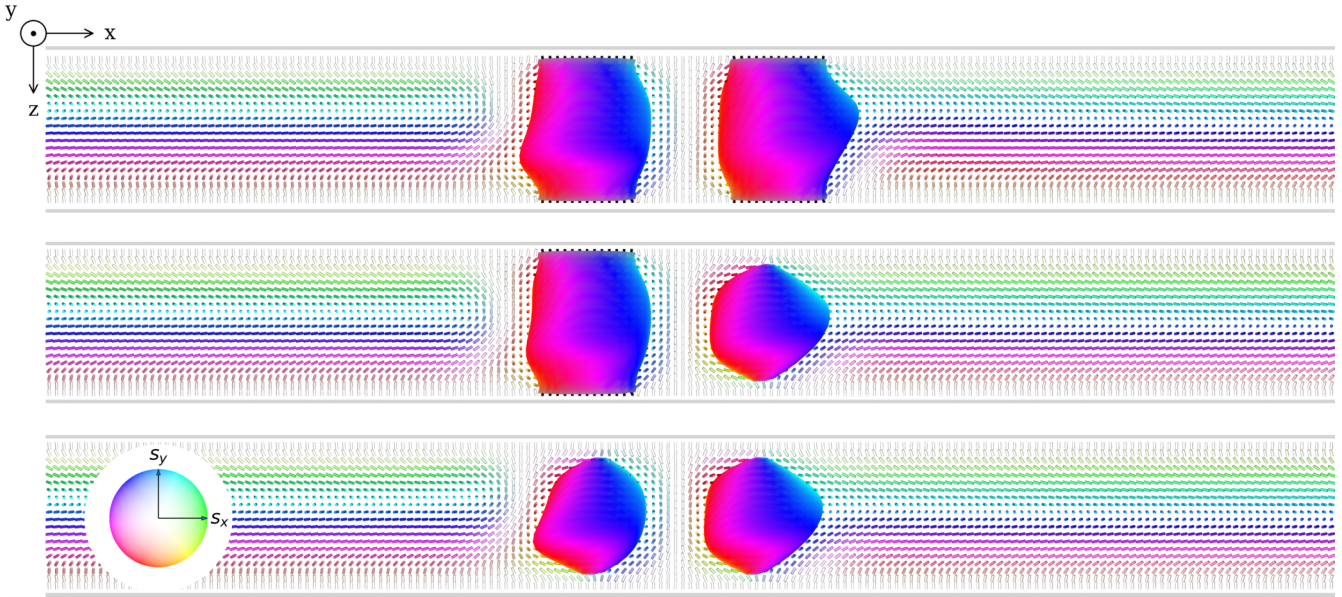


FIG. 4. Equilibrium two-soliton configurations for a pair of interacting skyrmion tubes (top), skyrmion-toron structure (middle), and toron-toron structure (bottom) in the chiral magnetic film or CLC cell (parameters and elements of visualization are explained in the caption of Fig. 1).

Although topological solitons are, in general, cylindrically (axially) asymmetric, the interaction potentials are found to be nearly insensitive to rotations of the intersoliton vector about the normal to the bounding surfaces (substrates). It agrees with the theoretical results of Refs. [18,48] and an important consequence of this is that both the skyrmion and toron lattices will be triangular.

Now we pass on to the interaction of the so-called leech states. As is shown in Fig. 2 (see, also, discussion in Sec. II), this structure is attached to one of the bounding surfaces of the film and looks like an intermediate state between the skyrmion tube and the toron. Since the film thickness only slightly exceeds the length of the leeches, the interaction between leeches located at different surfaces is strong enough to form two-leech structures. Therefore, for leeches, the diversity of interacting structures that depend on leech alignment is wider as compared to the skyrmion tubes and the torons.

We begin with the case of identically aligned leeches where the states are localized at the same film surface. The dependence of the interaction energy on the separation for a pair of leeches up is presented at the top of Fig. 5. It turns out that in contrast to the interaction of torons and skyrmions shown in Fig. 3, for leeches, the interaction is anisotropic and the interaction energy depends on the orientation of the

intersolitic separation vector. In Fig. 5, this orientation is specified by the angle  $\alpha$  between the lateral component of the separation vector and the vector that defines the spin or director far-field orientation of the background spiral structure in the middle of the film. Insets in Fig. 5 illustrate orientations of the interleech vector at  $\alpha \in \{0, \pm\pi/4, \pm3\pi/4, \pi\}$ . It can be seen that whatever the orientation of the interleech vector is, there is a local minimum of the interaction energy representing a locally stable structure. The corresponding spatial two-leech configuration is illustrated in Fig. 6 (top). The depth of the minimum typically depends on the orientation of the intersoliton vector and is less pronounced than that for both the skyrmion tubes and the torons.

Referring to Fig. 5 (top), variations of the results for the two-leech-up structures with  $\Delta\alpha = \pi$  are within the accuracy of the computations, whereas the cases of the interleech vector orientations with  $\alpha \in \{0, \pm\pi/4\}$  reveal noticeable differences. At  $\alpha = -\pi/4$  (the separation vector is along the  $y$  axis), the local minimum is deeper than in other directions. Therefore, it might be expected that a square lattice will be formed as the stable state at certain temperatures.

In this case, in addition to the local energy minimum, the interaction potential reaches the maximum located at about  $40a$ . This maximum appears to be suppressed at  $\alpha = 0$ , whereas it is shifted to the region of longer distances and located at about  $150a$  when  $\alpha = \pi/4$  (the separation vector is along the  $x$  axis). Note that in the presence of the maximum, the long-distance tail corresponds to the repulsive part of the potential.

When the intersoliton vector is along the  $y$  axis and the distance exceeds the leech transverse size, the interaction is stronger than both the interskyrmion and the intertoron interactions. In addition, a comparison between Figs. 4 and 6 shows that in the region where, for skyrmions and torons, the far-field spiral structure is undisturbed (see Fig. 4), the interleech interaction produces noticeable distortions of the

TABLE I. Binding energies of two-soliton and triple-soliton structures. Percents in brackets indicate the relative difference between the triple-soliton binding energy and the sum of pair interaction (two-soliton) energies associated with three (two) links of triangular (linear) configuration.

	Two-soliton structure	Triangular structure	Linear chain
Skyrmion	-11.46	-32.33 (6%)	-22.46 (2%)
Toron	-7.14	-17.34 (19%)	-14.28 (<1%)

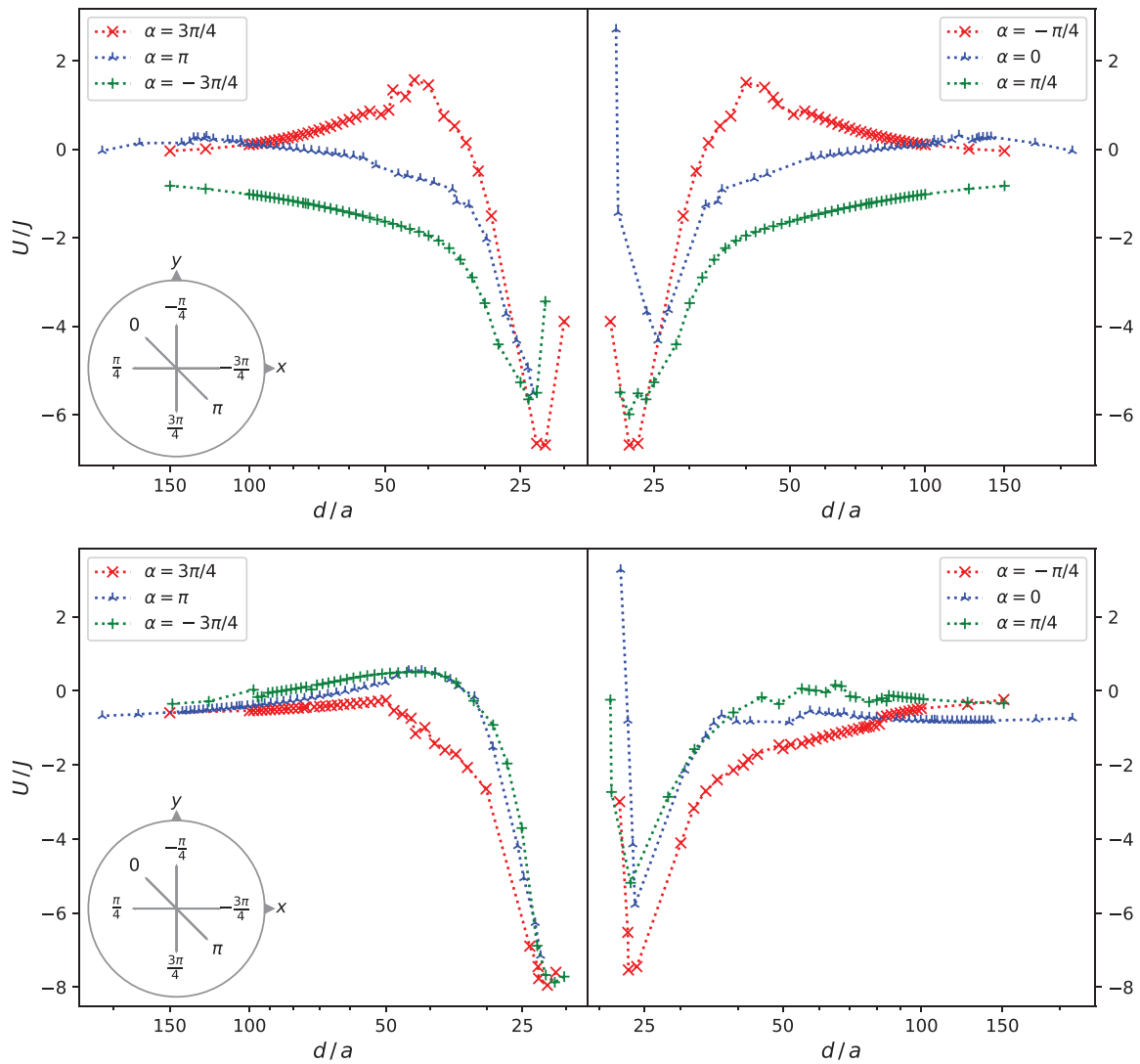


FIG. 5. Effective potential for pairwise interaction for identically aligned leeches (a pair of leeches up) (top) and for a leech up interacting with a leech down (bottom) at different values of the angle  $\alpha$  between the intersoliton separation vector connecting the centers of the leeches and the spin or director of the background structure in the middle of the sample. Insets illustrate how the interleech vector is aligned depending on the value of  $\alpha$ .

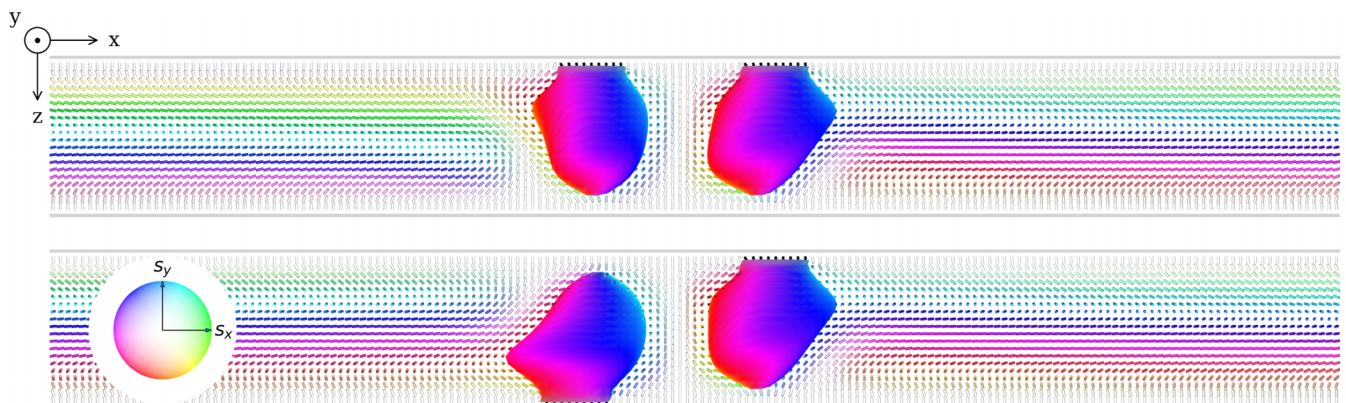


FIG. 6. Equilibrium states for two leeches up (top) and differently aligned leeches (bottom).



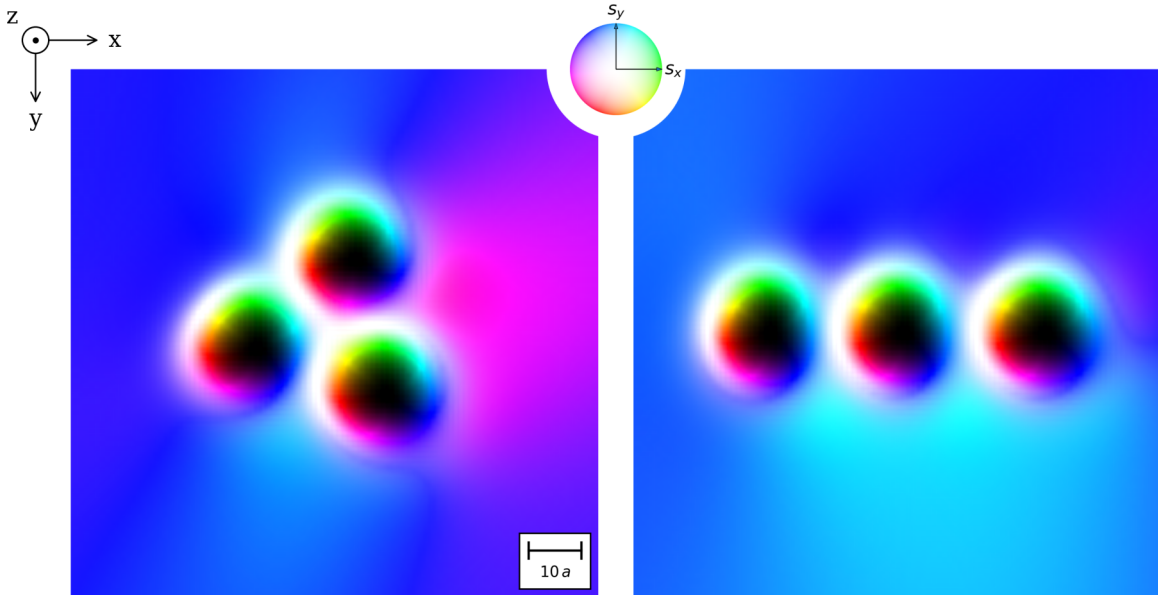


FIG. 7. Two three-skyrmion equilibrium configurations: the triangular structure (left) and the linear chain (right) in the chiral magnetic film or CLC cell (parameters and elements of visualization are explained in the caption of Fig. 1).

conical phase. Thus, we get the conclusion that the effective range of the interleech interaction is longer than the corresponding range of intersoliton interactions between skyrmions and torons.

For differently aligned leeches, the interleech interaction potentials of the two-leech up-down structure computed at  $\alpha \in \{0, \pm\pi/4, \pm3\pi/4, \pi\}$  are depicted in Fig. 5 (bottom). The two-leech configuration at the distance corresponding to the interaction energy minimum is shown in Fig. 6 (bottom).

At  $\alpha = 0$  and  $\alpha = \pi/4$ , the separation dependence of the interaction energy exhibits a bit less pronounced maximum as compared to the case of identically aligned leeches with  $\alpha = -\pi/4$ . When the lateral component of the interleech vector is along the  $y$  axis ( $\alpha = -\pi/4$ ), the maximum is suppressed and the long-distance part of the interaction is attractive.

It turns out that when the leeches are attached to different substrates, the interaction energy is no longer symmetric with respect to rotations about the  $z$  axis by  $\pi$  when the lateral component of the intersoliton vector changes its sign. In particular, from Fig. 5 (bottom), the difference between the energy maxima located on different sides of the reference structure is clearly seen.

#### IV. THREE-PARTICLE INTERACTION

As we have discussed in the previous section, the interaction between localized structures such as skyrmions and torons is attractive at sufficiently large separations. Therefore, it can be expected that these solitons will form ordered stable clusters determined by the pair interaction.

We have found that there are stable triple-soliton structures forming regularly shaped clusters of three solitons located at distances close to pairwise equilibrium. For skyrmions, Fig. 7 illustrates triangular and linearly ordered structures. The binding energies of skyrmion and toron structures, computed as the difference between the energy

of the three-soliton configuration and the sum of single-soliton energies, are listed in Table I. It is seen that the skyrmion clusters are energetically favorable over the toron ones.

From Table I, a comparison between the sum of pair interaction energies and the three-soliton binding energy shows that pairwise interactions are the determining factors for linear chains of skyrmions and torons. For the solitons arranged in a regular triangle, the accuracy of the pairwise approximation is not good and breaks down in the case of torons, indicating the presence of the noticeable contribution coming from the three-body interaction.

#### V. CONCLUSIONS

In this paper, we have used the lattice model describing chiral magnetism and CLC systems confined in the slab geometry to study intersoliton interactions between a variety of topological structures coexisting at certain values of the surface and bulk anisotropies (the homeotropic anchoring energy strength and external magnetic field in the case of CLC cells). These structures include the skyrmion tubes, torons, and leeches (see Figs. 1 and 2).

The three-step minimization procedure detailed in Sec. III is employed to perform numerical analysis of the intersoliton interaction potentials that are plotted in relation to the separation (the intersoliton distance) in Figs. 3 and 5. For skyrmions and torons, all the potentials are found to be nearly cylindrically (axially) symmetric whose asymptotic behavior is determined by the attractive long-distance tails that can be fitted using the relation (3) previously derived for the skyrmion-skyrmion interaction potentials in Refs. [18,28–30,48]. Note that in reality, cylindrical symmetry is broken by the Dzyaloshinskii-Moriya interaction and the energy functional (2) is not invariant with respect to global rotations of the spins about the normal to the bounding surfaces.

Nevertheless, by contrast to the interleech potentials, the intersoliton potentials for skyrmions and torons appear to be symmetric, with the accuracy limited by the errors of discretization.

A feature shared by all the intersoliton interaction potentials is that there is a local minimum located at the equilibrium distance corresponding to the lowest-energy (equilibrium) two-soliton configuration (these structures are illustrated in Figs. 4 and 6). It is also found that in the case of the skyrmion-skyrmion interaction, there is an additional minimum representing a metastable state of the short-separated pair of skyrmion tubes.

For identically and differently aligned leeches, the results presented in Fig. 5 suggest sensitivity of the potential to orientation of the interleech separation vector. It is shown that at certain orientations of the vector, in contrast to the case of skyrmions and torons, the large-distance part of the

potential may become repulsive owing to the presence a local maximum.

When several localized topological solitons can exist simultaneously, they may form ordered structures depending on the pairwise interaction between them. According to Fig. 7, the three-skyrmion locally stable structures are arranged either in a regular triangle or in a linear chain. Similar results hold for the three-toron structures. From Table I, the binding energies of linearly ordered structures are determined by the contributions coming from the two-soliton interaction, whereas, for the triangular structure of torons, the contribution of the three-soliton interaction cannot be neglected.

#### ACKNOWLEDGMENT

The study was supported by the Russian Science Foundation Grant No. 22-22-00632.

- 
- [1] N. Nagaosa and Y. Tokura, Topological properties and dynamics of magnetic skyrmions, *Nat. Nanotechnol.* **8**, 899 (2013).
  - [2] U. K. Rössler, A. N. Bogdanov, and C. Pfleiderer, Spontaneous skyrmion ground states in magnetic metals, *Nature (London)* **442**, 797 (2006).
  - [3] R. Wiesendanger, Nanoscale magnetic skyrmions in metallic films and multilayers: A new twist for spintronics, *Nat. Rev. Mater.* **1**, 16044 (2016).
  - [4] P. J. Ackerman and I. I. Smalyukh, Diversity of Knot Solitons in Liquid Crystals Manifested by Linking of Preimages in Torons and Hopfions, *Phys. Rev. X* **7**, 011006 (2017).
  - [5] I. I. Smalyukh, Review: Knots and other new topological effects in liquid crystals and colloids, *Rep. Prog. Phys.* **83**, 106601 (2020).
  - [6] I. Mušević, Interactions, topology and photonic properties of liquid crystal colloids and dispersions, *Eur. Phys. J.: Spec. Top.* **227**, 2455 (2019).
  - [7] B. Göbel, I. Mertig, and O. A. Tretiakov, Beyond skyrmions: Review and perspectives of alternative magnetic quasiparticles, *Phys. Rep.* **895**, 1 (2021).
  - [8] J.-S. Wu and I. I. Smalyukh, Hopfions, heliknotons, skyrmions, torons and both Abelian and non-Abelian vortices in chiral liquid crystals, *Liq. Cryst. Rev.* (2022), doi:10.1080/21680396.2022.2040058.
  - [9] V. M. Kuchkin, N. S. Kiselev, F. N. Rybakov, I. S. Lobanov, S. Blügel, and V. M. Uzdin, Heliknoton in a film of cubic chiral magnet, *Front. Phys.* **11**, 1201018 (2023).
  - [10] A. Fert, N. Reyren, and V. Cros, Magnetic skyrmions: Advances in physics and potential applications, *Nat. Rev. Mater.* **2**, 17031 (2017).
  - [11] *Magnetic Skyrmions and Their Applications*, Woodhead Publishing Series in Electronic and Optical Materials, edited by G. Finocchio and C. Panagopoulos (Elsevier, Duxford, UK, 2021), p. 451.
  - [12] J. H. Han, *Skyrmions in Condensed Matter*, Springer Tracts in Modern Physics Vol. 278 (Springer, New York, 2017), p. 177.
  - [13] *Skyrmions: Topological Structures, Properties, and Applications*, Series in Materials Science and Engineering, edited by J. P. Liu, Z. Zhang, and G. Zhao (CRC Press, Boca Raton, FL, 2017), p. 481.
  - [14] K. Everschor-Sitte, J. Masell, R. M. Reeve, and M. Kläui, Perspective: Magnetic skyrmions—Overview of recent progress in an active research field, *J. Appl. Phys.* **124**, 240901 (2018).
  - [15] I. M. Tambovtsev, A. O. Leonov, I. S. Lobanov, A. D. Kiselev, and V. M. Uzdin, Topological structures in chiral media: Effects of confined geometry, *Phys. Rev. E* **105**, 034701 (2022).
  - [16] F. Zheng, F. N. Rybakov, A. B. Borisov, D. Song, S. Wang, Z. A. Li, H. Du, N. S. Kiselev, J. Caron, A. Kovács, M. Tian, Y. Zhang, S. Blügel, and R. E. Dunin-Borkowski, Experimental observation of chiral magnetic bobbers in B20-type FeGe, *Nat. Nanotechnol.* **13**, 451 (2018).
  - [17] S. Schneider, D. Wolf, M. J. Stolt, S. Jin, D. Pohl, B. Rellinghaus, M. Schmidt, B. Büchner, S. T. B. Goennenwein, K. Nielsch, and A. Lubk, Induction Mapping of the 3D-Modulated Spin Texture of Skyrmions in Thin Helimagnets, *Phys. Rev. Lett.* **120**, 217201 (2018).
  - [18] D. Foster, C. Kind, P. J. Ackerman, J.-S. B. Tai, M. R. Dennis, and I. I. Smalyukh, Two-dimensional skyrmion bags in liquid crystals and ferromagnets, *Nat. Phys.* **15**, 655 (2019).
  - [19] S. S. Choi, S. M. Morris, W. T. S. Huck, and H. J. Coles, Electrically tuneable liquid crystal photonic bandgaps, *Adv. Mater.* **21**, 3915 (2009).
  - [20] T. N. Orlova, R. I. Iegorov, and A. D. Kiselev, Light-induced pitch transitions in photosensitive cholesteric liquid crystals: Effects of anchoring energy, *Phys. Rev. E* **89**, 012503 (2014).
  - [21] H. K. Bisoyi and Q. Li, Light-directed dynamic chirality inversion in functional self-organized helical superstructures, *Angew. Chem., Intl. Ed.* **55**, 2994 (2016).
  - [22] R. S. Zola and Q. Li, in *Functional Organic and Hybrid Nanostructured Materials*, edited by Q. Li (Wiley, New York, 2018), Chap. 8, pp. 307–357.
  - [23] H. K. Bisoyi, T. J. Bunning, and Q. Li, Stimuli-driven control of the helical axis of self-organized soft helical superstructures, *Adv. Mater.* **30**, 1706512 (2018).

- [24] S. Heinze, K. von Bergmann, M. Menzel, J. Brede, A. Kubetzka, R. Wiesendanger, G. Bihlmayer, and S. Blügel, Spontaneous atomic-scale magnetic skyrmion lattice in two dimensions, *Nat. Phys.* **7**, 713 (2011).
- [25] A. O. Leonov, A. N. Bogdanov, and K. Inoue, Toggle-switch-like crossover between two types of isolated skyrmions within the conical phase of cubic helimagnets, *Phys. Rev. B* **98**, 060411(R) (2018).
- [26] A. O. Leonov, T. L. Monchesky, J. C. Loudon, and A. N. Bogdanov, Three-dimensional chiral skyrmions with attractive interparticle interactions, *J. Phys.: Condens. Matter* **28**, 35LT01 (2016).
- [27] A. O. Leonov, Surface anchoring as a control parameter for shaping skyrmion or toron properties in thin layers of chiral nematic liquid crystals and noncentrosymmetric magnets, *Phys. Rev. E* **104**, 044701 (2021).
- [28] B. M. A. G. Piette, B. J. Schroers, and W. J. Zakrzewski, Multisolitons in a two-dimensional skyrmion model, *Z. Phys. C-Particles Fields* **65**, 165 (1995).
- [29] D. Capic, D. A. Garanin, and E. M. Chudnovsky, Skyrmion-skyrmion interaction in a magnetic film, *J. Phys.: Condens. Matter* **32**, 415803 (2020).
- [30] C. Ross, N. Sakai, and M. Nitta, Skyrmion interactions and lattices in chiral magnets: Analytical results, *J. High Energy Phys.* **02** (2021) 95.
- [31] L. Rózsa, A. Deák, E. Simon, R. Yanes, L. Udvardi, L. Szunyogh, and U. Nowak, Skyrmions with Attractive Interactions in an Ultrathin Magnetic Film, *Phys. Rev. Lett.* **117**, 157205 (2016).
- [32] S. M. Vlasov, A. O. Leonov, and V. M. Uzdin, Skyrmion flop transition and congregation of mutually orthogonal skyrmions in cubic helimagnets, *J. Phys.: Condens. Matter* **32**, 185801 (2020).
- [33] H. R. O. Sohn, S. M. Vlasov, V. M. Uzdin, A. O. Leonov, and I. I. Smalyukh, Real-space observation of skyrmion clusters with mutually orthogonal skyrmion tubes, *Phys. Rev. B* **100**, 104401 (2019).
- [34] J. C. Loudon, A. O. Leonov, A. N. Bogdanov, M. C. Hatnean, and G. Balakrishnan, Direct observation of attractive skyrmions and skyrmion clusters in the cubic helimagnet  $\text{Cu}_2\text{OSeO}_3$ , *Phys. Rev. B* **97**, 134403 (2018).
- [35] H. Du, X. Zhao, F. N. Rybakov, A. B. Borisov, S. Wang, J. Tang, C. Jin, C. Wang, W. Wei, N. S. Kiselev, Y. Zhang, R. Che, S. Blügel, and M. Tian, Interaction of Individual Skyrmions in a Nanostructured Cubic Chiral Magnet, *Phys. Rev. Lett.* **120**, 197203 (2018).
- [36] I. I. Smalyukh, Liquid crystal colloids, *Annu. Rev. Condens. Matter Phys.* **9**, 207 (2018).
- [37] Y. Yuan, A. Martinez, B. Senyuk, M. Tasinkevych, and I. I. Smalyukh, Chiral liquid crystal colloids, *Nat. Mater.* **17**, 71 (2018).
- [38] S. Ramaswamy, R. Nityananda, V. A. Raghunathan, and J. Prost, Power-law forces between particles in a nematic, *Mol. Cryst. Liq. Cryst. Sci. Technol., Sect. A* **288**, 175 (1996).
- [39] R. W. Ruhwandl and E. M. Terentjev, Long-range forces and aggregation of colloid particles in a nematic liquid crystal, *Phys. Rev. E* **55**, 2958 (1997).
- [40] T. C. Lubensky, D. Pettey, N. Currier, and H. Stark, Topological defects and interactions in nematic emulsions, *Phys. Rev. E* **57**, 610 (1998).
- [41] B. I. Lev and P. M. Tomchuk, Interaction of foreign macrodroplets in a nematic liquid crystal and induced supermolecular structures, *Phys. Rev. E* **59**, 591 (1999).
- [42] B. I. Lev, S. B. Chernyshuk, P. M. Tomchuk, and H. Yokoyama, Symmetry breaking and interaction of colloidal particles in nematic liquid crystals, *Phys. Rev. E* **65**, 021709 (2002).
- [43] J.-i. Fukuda and S. Žumer, Confinement effect on the interaction between colloidal particles in a nematic liquid crystal: An analytical study, *Phys. Rev. E* **79**, 041703 (2009).
- [44] O. M. Tovkach, S. B. Chernyshuk, and B. I. Lev, Theory of elastic interaction between arbitrary colloidal particles in confined nematic liquid crystals, *Phys. Rev. E* **86**, 061703 (2012).
- [45] B. I. Lev, J.-i. Fukuda, O. M. Tovkach, and S. B. Chernyshuk, Interaction of small spherical particles in confined cholesteric liquid crystals, *Phys. Rev. E* **89**, 012509 (2014).
- [46] O. M. Tovkach, S. B. Chernyshuk, and B. I. Lev, Colloidal interactions in a homeotropic nematic cell with different elastic constants, *Phys. Rev. E* **92**, 042505 (2015).
- [47] V. M. Pergamenschchik, The model of elastic multipole, *J. Mol. Liq.* **267**, 337 (2018).
- [48] S. B. Chernyshuk and E. G. Rudnikov, Theory of elastic interaction between axially symmetric 3D skyrmions in confined chiral nematic liquid crystals and in skyrmion bags, *Liq. Cryst.* **50**, 9 (2023).
- [49] H. R. O. Sohn, C. D. Liu, and I. I. Smalyukh, Schools of skyrmions with electrically tunable elastic interactions, *Nat. Commun.* **10**, 4744 (2019).
- [50] A. O. Leonov, Skyrmion clusters and chains in bulk and thin-layered cubic helimagnets, *Phys. Rev. B* **105**, 094404 (2022).
- [51] F. N. Rybakov, A. B. Borisov, S. Blügel, and N. S. Kiselev, New spiral state and skyrmion lattice in 3D model of chiral magnets, *New J. Phys.* **18**, 045002 (2016).
- [52] J.-S. B. Tai and I. I. Smalyukh, Surface anchoring as a control parameter for stabilizing torons, skyrmions, twisted walls, fingers, and their hybrids in chiral nematics, *Phys. Rev. E* **101**, 042702 (2020).
- [53] W. Legrand, D. Maccariello, F. Ajejas, S. Collin, A. Vecchiola, K. Bouzehouane, N. Reyren, V. Cros, and A. Fert, Room-temperature stabilization of antiferromagnetic skyrmions in synthetic antiferromagnets, *Nat. Mater.* **19**, 34 (2020).
- [54] J. Müller, A. Rosch, and M. Garst, Edge instabilities and skyrmion creation in magnetic layers, *New J. Phys.* **18**, 065006 (2016).
- [55] S.-Z. Lin, C. Reichhardt, C. D. Batista, and A. Saxena, Particle model for skyrmions in metallic chiral magnets: Dynamics, pinning, and creep, *Phys. Rev. B* **87**, 214419 (2013).